



Synthesis, characterization and biological activity of copper(II) complexes with ligands derived from β -amino acids

Andriana M. Bukonjić¹ · Dušan Lj. Tomović¹ · Ana S. Stanković¹ · Verica V. Jevtić² · Zoran R. Ratković² · Jovana V. Bogojeski² · Jelena Z. Milovanović³ · Dragana B. Đorđević³ · Aleksandar N. Arsenijević³ · Marija Z. Milovanović³ · Ivan Potočňák⁴ · Srećko R. Trifunović² · Gordana P. Radić¹

Received: 12 June 2018 / Accepted: 2 August 2018
© Springer Nature Switzerland AG 2018

Abstract

Two copper(II) complexes with ligands derived from β -amino acids, 2-(1-aminocyclohexyl)acetic acid **L1** and 2-(1-amino-4-(*tert*-butyl)cyclohexyl)acetic acid **L2**, were synthesized and characterized by microanalysis, infrared, UV–Vis and EPR spectra. The spectroscopically predicted structure of the square-planar copper(II) complex with 2-(1-aminocyclohexyl)-acetic acid **C1** was confirmed by single-crystal X-ray analysis. The biological activities (antitumor activities and interaction with DNA) of the compounds were also investigated. The interactions of both complexes with calf thymus (CT) and herring testes (HT) DNA were examined by stopped-flow spectroscopy, by absorption (UV–Vis) and by emission spectral studies (ethidium bromide displacement studies). Both complexes were found to react a bit faster with HT-DNA than with CT-DNA. The obtained binding constants suggested a moderate intercalative binding mode between the complexes and DNA. In addition, fluorescence spectrometry of bovine serum albumin with the complexes showed a good fluorescence quenching of the complexes. The obtained copper(II) complexes have a relatively low cytotoxic effect on murine mammary carcinoma cell line, 4T1, a moderate effect on murine colon carcinoma cell line, CT26, and a relatively high cytotoxicity toward murine lung cancer cells, LLC1.

Electronic supplementary material The online version of this article (<https://doi.org/10.1007/s11243-018-0270-0>) contains supplementary material, which is available to authorized users.

✉ Jovana V. Bogojeski
jrosic@kg.ac.rs

✉ Gordana P. Radić
vasic_gordana@yahoo.com

¹ Department of Pharmacy, Faculty of Medical Sciences, University of Kragujevac, Svetozara Markovića 69, Kragujevac 34000, Republic of Serbia

² Department of Chemistry, Faculty of Science, University of Kragujevac, Radoja Domanovića 12, Kragujevac 34000, Republic of Serbia

³ Department of Microbiology and Immunology, Center for Molecular Medicine and Stem Cell Research, Faculty of Medical Sciences, University of Kragujevac, Svetozara Markovića 69, Kragujevac 34000, Republic of Serbia

⁴ Institute of Chemistry, P.J. Šafárik University, Moyzesova 11, 041 54 Kosice, Slovakia

Introduction

Copper is a trace element, but it plays a very important role in all living organisms. Thus, it participates in redox reactions, in growth and development of organisms, and is a component of numerous enzymes [1]. A deviation from homeostatic copper concentrations can lead to the development of various diseases, including Wilson's disease and Menkes disease, and is also thought to be responsible for malignant angiogenesis, i.e., invasiveness of tumor cells and the onset of metastases [1–4].

The biological activity of transition metal complexes is increasingly attracting researchers' attention with the aim of finding potential pharmacotherapeutics [5, 6]. In this context, copper(II) complexes have also been investigated, but with an insufficiently clear mechanism of action [5, 7]. Previous investigations have shown that the properties of copper complexes mainly depend on the nature of the ligands and their donor atoms, but also on the differences in activities of the copper(I) and copper(II) complexes [7]. In general, coordination of copper(II) is realized through oxygen, nitrogen, sulfur and phosphorus donor ligands. Copper(II) complexes

can show a significant cytotoxic activity for ligands that contain polydentate Schiff bases, five-membered aromatic heterocycles (imidazole, pyrazole, triazole) or six-membered aromatic heterocycles such as bipyridine (bipy) or tertiary phosphines [1, 4]. These complexes lead to the inhibition of *Staphylococcus aureus* and *Escherichia coli* [8], while the introduction of several different heterocyclic bases increases the microbial spectrum of the effect [9, 10].

Recent studies are increasingly being focused on the synthesis of complexes of α -amino acid ligands and their derivatives. These include the study of the stability of such complexes, their binding to DNA, and their biological activities [11–16]. A copper(II) complex of bacitracin showed a significant oxidative activity [16]. The comparative analysis of three complexes of copper(II) with glycine (gly), alanine (ala) and a combination of ligands (gly and bipy) showed that the complex with both amino acid and heterocyclic ligands showed the strongest interaction with DNA and the highest cytotoxic activity [12].

Based on previously published results, we can conclude that, in general, β -amino acids show better biological activities in comparison with α -amino acids [17–19]. We reasoned that if such β -amino acids were in the coordination sphere of copper(II), the biological activities of the resulting complexes might be better still. Because this area has not yet been fully explored, in this paper our investigations are focused on the synthesis of copper(II) complexes of derivatives of β -amino acids, namely 2-(1-aminocyclohexyl)acetic acid **L1** and 2-(1-amino-4-(*tert*-butyl)cyclohexyl)-acetic acid **L2** as well as the biological activities (antitumor activities and interactions with DNA) of the obtained compounds. The structures of the complexes were deduced on the basis of elemental microanalysis and infrared spectra; moreover, the square-planar structure was confirmed by an X-ray structural study of the copper(II) complex of **L1**. The interactions of the copper(II) complexes with CT-DNA and HT-DNA were investigated. Since it is considered that some transition metal complexes manifest their antitumor activity by interactions with certain proteins [20, 21], we considered it important to examine the affinity of these new complexes with a protein, namely bovine serum albumin (BSA). In this study, we report on the cytotoxicities of the two proligands and their corresponding copper(II) complexes against murine colon carcinoma cell line, CT26, murine mammary carcinoma cells line, 4T1, and murine lung cancer cell line, LLC1.

Experimental

Materials and measurements

All reagents were obtained commercially and used without further purification. Elemental analyses were obtained on a

Vario III CHNOS Elemental Analyzer, Elemental Analysensysteme GmbH. For infrared spectra, a PerkinElmer FTIR 31725-X spectrophotometer and KBr pellet technique were employed.

The 9.8 GHz EPR spectra were recorded at room temperature on a Bruker Eleksys II 540 EPR spectrometer under the following conditions: microwave power 6.325 mW, modulation amplitude 5 G, modulation frequency 100 kHz, conversion time 240 ms. The samples (30 μ L of 0.5 mM aqueous solution, in deionized 18 M Ω water) were drawn into gas-permeable Teflon tubes (Zeus industries, Raritan, NJ). The spectra were recorded and analyzed using the Bruker Xepr software.

Kinetics of the substitution reactions of the copper(II) complexes with CT and HT-DNA were studied in a stopped-flow spectrophotometer (PerkinElmer Lambda 35) in 25 mM Hepes buffer, pH \approx 7.2 (Acros Organics, Belgium).

Syntheses

Synthesis of proligands

The proligands, 2-(1-aminocyclohexyl)acetic acid **L1** and 2-(1-amino-4-(*tert*-butyl)cyclohexyl)acetic acid **L2**, were obtained by using the previously described process [22]. A mixture of cyclohexanone or 4-*tert*-butyl-cyclohexanone (1 mol), malonic acid (1 mol) and ammonium acetate (1 mol) in 1-butanol (600 mL) was refluxed for 1.5–3.0 h until CO₂ was no longer evolved. The postreaction mixtures were transparent solutions. All volatile compounds boiling to 135 °C were distilled off; a colorless film of ammonium malonate was deposited in the Liebig condenser. The reaction mixture was diluted with 1-butanol (300 mL), and the distillation was repeated. The residue was distilled in a vacuum of 10–20 mmHg, until the boiling point of the distillate reached 128–130 °C. The resulting viscous oil was cooled to 20 °C and stirred with acetone (700 mL). Afterward it was allowed to stand for no less than 10 h, and the resulting amino acid precipitates were filtered off, washed with acetone and dried at 100 °C.

2-(1-aminocyclohexyl)acetic acid (L1) IR (KBr, cm⁻¹): 3424 (w), 2945 (s), 2166 (w), 1619 (s), 1570 (s), 1492 (m), 1467 (m), 1383 (m), 1266 (w), 1200 (w), 1133 (w), 1060 (w), 946 (w), 899 (w), 764 (w), 717 (w), 603 (w). ¹H NMR (200 MHz, CDCl₃, δ ppm): 1.25–1.47 (m, 6H, 3CH₂), 1.47–1.58 (m, 4H, 2CH₂), 2.09 (s, 2H, CH₂). ¹³C NMR (50 MHz, CDCl₃, δ ppm): 42.5 (C–), 48.0 (CH₂– from acetic acid); 41.2; 21.9; 22.6 (CH₂– from cyclohexyl group); 177.3 (COOH).

2-(1-amino-4-(*tert*-butyl)cyclohexyl)acetic acid (L2) IR (KBr, cm⁻¹): 3433 (w), 2954 (s), 2153 (w), 1639 (s), 1583

(s), 1506 (m), 1466 (m), 1395 (m), 1364 (m), 1336 (m), 1262 (w), 1173 (w), 1055 (w), 950 (w), 901 (w), 764 (w), 714 (w), 623 (w). ^1H NMR (200 MHz, CDCl_3 , δ ppm): 2.41 (s, 2H, CH_2), 1.52–1.75 (m, 8H, 4 CH_2), 1.41 (s, H, CH), 0.49 (m, 9H, 3 CH_3). ^{13}C NMR (50 MHz, CDCl_3 , δ ppm): 42.8 (C-from cyclohexyl group), 48.0 (CH_2 - from acetic acid); 20.7; 39.6 (CH_2 - from cyclohexyl group); 32.5 (CH-from cyclohexyl group); 27.6 (CH_3 - from *t*-butyl group); 177.3 (COOH).

Synthesis of the complexes

Copper(II) nitrate trihydrate (0.1000 g, 0.4139 mmol) was dissolved in water (10.0 mL) on a steam bath, and 2-(1-aminocyclohexyl)acetic acid **L1** (0.1301 g, 0.8278 mmol) or 2-(1-amino-4-(*tert*-butyl)cyclohexyl)acetic acid **L2** (0.1766 g, 0.8278 mmol) was added. The reaction mixture was heated for 3 h, and during this period 10.0 mL of an aqueous lithium hydroxide solution (0.0199 g, 0.8278 mmol) was added in small portions. The solutions were filtered and evaporated to small volume.

Single crystals of the copper(II) complex with 2-(1-aminocyclohexyl)acetic acid (**C1**) suitable for single-crystal X-ray diffraction analysis were obtained by slow evaporation of a water solution. Yield: 0.1256 g (80.75%). *Anal.* Calc. for **C1** = $\text{CuC}_{16}\text{H}_{28}\text{N}_2\text{O}_4$ ($M_r = 375.95$): C, 51.12; H, 7.51; N, 7.45%. Found: C, 51.27; H, 7.42; N, 7.42%. IR (KBr, cm^{-1}): 3375 (s), 3293 (s), 3243 (s), 2933 (m), 2865 (m), 1576 (s), 1408 (s), 1375 (s), 1198 (m), 1139 (w), 1065 (w), 957 (w), 804 (w), 730 (w), 678 (w).

Complex (**C2**) was obtained as a blue powder from a water solution by slow evaporation. Yield: 0.1581 g (78.24%). *Anal.* Calc. for **C2** = $\text{CuC}_{24}\text{H}_{44}\text{N}_2\text{O}_4$ ($M_r = 488.16$): C, 59.05; H, 9.08; N, 5.74%. Found: C, 58.98; H, 9.01; N, 5.69%. IR (KBr, cm^{-1}): 3369 (s), 3297 (s), 3239 (s), 2949 (m), 2866 (m), 1577 (s), 1448 (s), 1429 (s), 1408 (s), 1326 (s), 1209 (m), 1176 (m), 1121 (w), 1109 (w), 993 (w), 973 (w), 959 (w), 900 (w), 733 (w), 680 (w).

Single-crystal X-ray crystallography

A summary of the X-ray diffraction experiment and structure refinement for **C1** is given in Table S1. The crystal structure of **C1** was determined using an Oxford Diffraction Xcalibur2 diffractometer equipped with a Sapphire2 CCD detector using graphite monochromated Mo $\text{K}\alpha$ radiation ($\lambda = 0.71073 \text{ \AA}$). CrysAlis CCD [23] was used for data collection, while CrysAlis RED [23] was used for cell refinement, data reduction and absorption correction. The structure was solved by SUPERFLIP [24] and subsequent Fourier syntheses using SHELXL2013 [25], as implemented in the WinGX program suite [26]. Anisotropic displacement parameters were refined for all non-H atoms. Hydrogen atoms from the

water molecules were found in the difference Fourier map and refined using a riding model; all other hydrogen atoms were placed in calculated positions and refined riding on their parent C or N atoms. An analysis of bond distances and angles was performed using SHELXL2013. DIAMOND [27] was used for molecular graphics.

Kinetic measurements

The interactions of complexes **C1** and **C2** with CT- and HT-DNA were studied by stopped-flow spectroscopy. In a typical experiment, one syringe contained various concentrations of CT- or HT-DNA in PBS buffer (pH = 7.2), and the other contained 1.0 mM of complex **C1** or **C2**. For each run, equal volumes of both solutions from separate syringes were rapidly mixed in the mixing chamber and the changes in absorbance were monitored for a chosen period of time. The temperature of both drive syringes, the cell and the mixing chamber was maintained at $37.0 \pm 0.2 \text{ }^\circ\text{C}$ using a circulating water bath. The absorbance change was measured at $\lambda = 260 \text{ nm}$ after the addition of either complex. The observed *pseudo*-first-order rate constants, k_{obsd} , were calculated as the average values from four to six independent kinetic runs using the program OriginPro 8. Experimental data are presented in Tables S2–S5.

DNA interactions

Stock solutions of CT-DNA and HT-DNA were prepared in PBS buffer. The ratio of UV absorbances at 260 and 280 nm (A_{260}/A_{280}) of ca. 1.8–1.9 indicated that the DNA was sufficiently free from protein. The concentration was determined by the UV absorbance at 260 nm ($\epsilon = 6600 \text{ M}^{-1} \text{ cm}^{-1}$) [28]. The UV–Vis spectra were obtained on a PerkinElmer Lambda 35 or 25 double beam spectrophotometer, using 1.0 cm path length quartz cuvettes (3.0 mL). Fluorescence measurements were taken on an RF-1501 PC spectrofluorometer (Shimadzu, Japan). The fluorescence spectra were recorded in the range of 550–750 nm upon excitation at 527 nm in all cases. The excitation and emission bandwidths were both 10 nm.

UV–Vis absorption studies

In order to compare the binding strengths of the complexes with DNA, the intrinsic binding constants K_b were determined by monitoring the changes in absorption at the MLCT band with increasing concentrations of CT-DNA, using the following Eq. 1;

$$[\text{DNA}]/(\epsilon_A - \epsilon_f) = [\text{DNA}]/(\epsilon_b - \epsilon_f) + 1/[K_b(\epsilon_b - \epsilon_f)] \quad (1)$$

where K_b is given by the ratio of slope to the y intercept in plots of $[\text{DNA}]/(\epsilon_A - \epsilon_f)$ versus $[\text{DNA}]$, where $[\text{DNA}]$

is the concentration of DNA in the base pairs, $\varepsilon_A = A_{\text{obsd}}/[\text{complex}]$, ε_f is the extinction coefficient for the unbound complex, and ε_b is the extinction coefficient for the complex in the fully bound form.

Ethidium bromide (EB) displacement studies

The binding strengths of complexes to CT-DNA and HT-DNA were determined by calculating the quenching constant (K_{sv}) from the slopes of straight lines obtained from the Stern–Volmer equation (Eq. 2).

$$I_0/I = 1 + K_{sv}[Q] \quad (2)$$

where I_0 and I represent the emission intensities in the absence and the presence of the quencher (complex **C1** or **C2**), respectively; $[Q]$ is a total concentration of quencher; K_{sv} is the Stern–Volmer quenching constant which can be obtained from the slope of the plot of I_0/I versus $[Q]$.

Viscosity measurements

The viscosity of DNA solutions was measured in the presence of increasing amounts of complexes **C1** and **C2**. The flow time was measured with a digital stopwatch. Each sample was measured three times, and the average flow time was calculated. The data are presented as $(\eta/\eta_0)^{1/3}$ against r , where η is the viscosity of DNA in the presence of the complex and η_0 is the viscosity of DNA alone in the buffer solution. The viscosity values were calculated from the observed flow time of the DNA-containing solutions (t), corrected for the flow time of the buffer alone (t_0), $\eta = (t - t_0)/t_0$.

In vitro cytotoxicity studies

The complexes were dissolved in 10% DMSO in distilled water at a concentration of 10 mM and filtered through a 0.22-mm Millipore filter. These stock solutions were diluted in culture medium immediately before use. MTT (3-(4,5-dimethylthiazol-2-yl)-2,5-diphenyl tetrazolium bromide) was dissolved (5 mg/mL) in a phosphate buffer saline having a pH of 7.2 and filtered through a 0.22-mm Millipore filter before use. All reagents were purchased from Sigma Chemicals.

CT26, 4T1 and LLC1 cells were purchased from the American Type Culture Collection (ATCC, Manassas, USA). The cells were maintained in DMEM (Sigma-Aldrich, Munich, Germany) supplemented with 10% fetal bovine serum (FBS, Sigma-Aldrich, Munich, Germany), penicillin (100 IU/mL) and streptomycin (100 $\mu\text{g}/\text{mL}$) in a humidified atmosphere of 95% air/5% CO_2 at 37 °C. Subconfluent monolayers, in log growth phase, were harvested by brief treatment with 0.25% trypsin and 0.02% EDTA in phosphate buffered saline (PBS, Sigma-Aldrich, Munich, Germany) and washed three times in

serum-free PBS. The number of viable cells was determined by trypan blue exclusion.

The effects of the test compounds on cell viability were determined using the MTT colorimetric technique [29]. Cells were diluted in growth medium to (5×10^4 cells/mL), and aliquots (5×10^3 cells/100 mL) were placed in individual wells in 96 multiplates. The next day, the medium was exchanged with 100 μL solution of the test compounds, which had been serially diluted twofold in the medium such that concentrations ranged from 1000 to 7.8 μM in growth medium. Each compound was tested in triplicate. The cells were incubated at 37 °C in 5% CO_2 for 72 h. After the incubation, the supernatant was removed and 15% MTT solution (5 mg/mL in PBS, 10 μL) in DMEM medium without FBS was added to each well. After an additional 4 h of incubation at 37 °C in a 5% CO_2 , the medium with MTT was removed and DMSO (150 μL) with glycine buffer (20 μL) was added to dissolve the crystals. The plates were shaken for 10 min. The optical density of each well was determined at 595 nm using a microplate Zenyth 3100 Multimode detector. The percentage of cytotoxicity was calculated as a percentage using the formula:

$$\% \text{ cytotoxicity} = 100 - ((E - B)/(S - B) \times 100)$$

where B is for the background medium alone, S is for total viability/spontaneous death of untreated target cells, and E is for the experimental well. All experiments were carried out in triplicate.

For the apoptosis assays, the cells were plated in T25 culture flasks and allowed to grow overnight. After the cells reached subconfluency, the medium was replaced with the complex (15 μM). The exposed cells were kept at 37 °C in a 5% CO_2 incubator for 24 h. The cultured cells were washed twice with PBS and resuspended in 1 \times binding buffer (10 \times binding buffer: 0.1 M HEPES/NaOH (pH 7.4), 1.4 M NaCl, 25 mM CaCl_2) at a concentration $1 \times 10^6/\text{mL}$. Annexin FITC and propidium iodide (PI) were added to 100 mL of cell suspension and incubated for 15 min at room temperature (25 °C) in the dark. After the incubation, 400 mL of 1 \times binding buffer was added to each tube and the stained cells were analyzed within 1 h by using FACS Calibur (BD, San Jose, USA) and Flow Jo software (Tri Star). Since Annexin V FITC staining precedes the loss of membrane integrity that accompanies the later stage identified by PI, Annexin FITC positive, PI negative indicates early apoptosis, while the viable cells are Annexin V FITC negative, PI negative. Cells that are in late apoptosis or already dead are both Annexin V FITC and PI positive.

Results and discussion

Synthesis and chemical characterization

Two β -amino acids derivatives 2-(1-aminocyclohexyl)acetic acid **L1** and 2-(1-amino-4-(*tert*-butyl)cyclohexyl)acetic acid **L2** were prepared [22] by direct reaction of cyclohexanone, malonic acid and ammonium acetate. The corresponding copper(II) complexes **C1** and **C2** were obtained by direct reaction of copper(II) nitrate with **L1** and **L2**, respectively, in a molar ratio of 1:2, followed addition of an equimolar amount of aqueous lithium hydroxide, with satisfactory yields of about 80% (Scheme 1).

Infrared spectra of the isolated complexes were recorded in order to identify the coordination mode of β -amino acids ligands. In particular, the asymmetric stretching frequencies of the carboxylic groups were used to determine whether these groups were uncoordinated (absorption bands expected in the range from 1700 to 1750 cm^{-1}) or coordinated (absorption bands are located in the range from 1600 to 1650 cm^{-1}) to the metal center [30–32]. Thus, the isolated copper(II) complexes both show double sharp and strong asymmetric stretching frequencies of the carboxylic groups at about 1650–1570 cm^{-1} . The observed clear double bands for the complexes suggest small differences in coordination of the ligand carboxylic groups to the metal.

The infrared spectra of both complexes confirm a bidentate mode by means of the amino nitrogen atoms. The isolated copper(II) complexes show asymmetric stretching frequencies of the primary amino group at 3375 cm^{-1} for **C1** and 3369 cm^{-1} for **C2**. Also, the complexes have no absorption bands from protonic amino groups, whereas in the spectra-free amino acids the signals of the protonic amino group appear at about 3300–2300 cm^{-1} (specifically 2944 cm^{-1} **L1** and 2954 cm^{-1} **L2**).

Based on the composition of the complexes and their IR spectra alone, it cannot be concluded with certainty how the β -amino acid derivatives are coordinated to copper(II). However, a single-crystal X-ray diffraction study of complex **C1** revealed that the metal is coordinated to **L1** in a square-planar copper(II) complex with *trans(O)-trans(N)*-geometry. Since ligand **L2** is a structural analog of **L1**, a similar geometry can be expected for the structure of corresponding copper(II) complex **C2**.

The electronic spectra of both complexes were recorded in water, with a concentration of 1×10^{-4} mol/dm³ at room temperature. The spectra show an absorption band at 264 nm for **C1** and at 256 nm for **C2**.

Figure 1 shows room temperature EPR spectra of the two copper(II) complexes in 0.5 mM aqueous solution. Both spectra are anisotropic with axial symmetry and clearly show different Cu signals, most likely due to the different ligands. The spectrum of complex **C1** is characterized by $g_{\parallel} = 2.16$, and $g_{\perp} = 2.07$. The spectrum of complex **C2** shows a poorly resolved Cu signal ($S = 1/2$, $I = 3/2$) hyperfine coupling, with $g_{\parallel} = 2.23$, and $g_{\perp} = 2.09$.

Scheme 1 Synthesis of **L1** (R = H) and **L2** (R = *tert*-butyl) and the corresponding complexes **C1** and **C2**

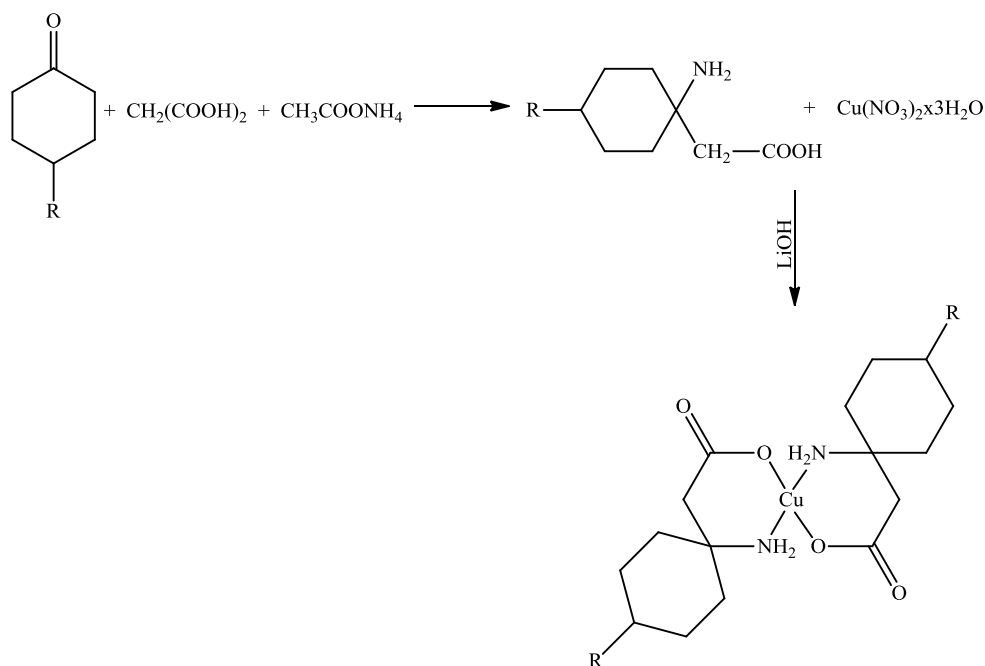


Fig. 1 Room temperature X-band EPR spectra of complexes **a** **C1** and **b** **C2** in water (0.5 mM)

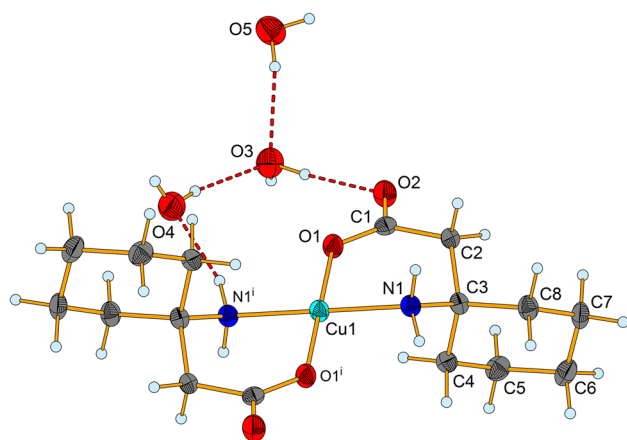
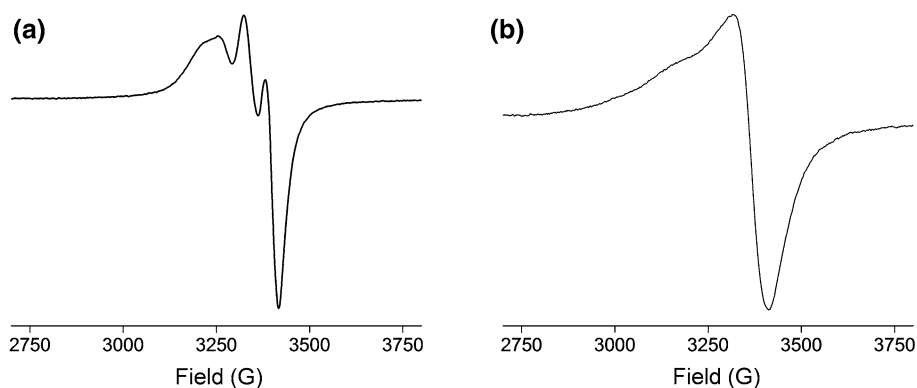


Fig. 2 Molecular structure of **C1** with thermal ellipsoids shown at 40% probability. Dashed lines represent hydrogen bonds ($i: -x+1, -y, -z+1$)

Crystal structure of complex **C1**

The X-ray crystal structure of **C1**, shown in Fig. 2, reveals a neutral complex molecule consisting of a Cu(II) atom and two bidentate **L1** ligands. These are coordinated to Cu1 by their O1 atoms after deprotonation of the carboxylic groups, and by their amino N1 atoms in *trans*-positions forming a square-planar coordination sphere around Cu1. As the Cu1 atom is localized at the center of symmetry, the complex unit contains only one independent **L1** ligand.

The selected bond lengths and angles for **C1** are summarized in Table 1. A deformed square-planar geometry around the central atom is confirmed by the N1–Cu1–O1 and N1–Cu1–O1ⁱ bite angles ($i = 1 - x, -y, 1 - z$) which differ a little from 90° as expected for atoms coordinated in *cis*-positions, and also by the Cu1–O1 bond which is slightly shorter than the Cu1–N1 bond due to the smaller covalent radius of oxygen. Nevertheless, the bond distances around the Cu1 atom are similar to those observed in twelve similar Cu(II) complexes with different β -amino acids as reported in the Cambridge Structure Database

Table 1 Selected bond lengths (Å) and angles [°] for **C1**

Cu1–O1	1.9238(15)	O1–Cu1–N1 ⁱ	87.45(7)
Cu1–N1	1.9852(17)	O1 ⁱ –Cu1–N1	87.45(7)
O1–C1	1.280(3)	O1–Cu1–N1	92.55(7)
O2–C1	1.245(3)	C1–O1–Cu1	130.35(14)
N1–C3	1.500(3)	C3–N1–Cu1	113.79(13)
C1–C2	1.520(3)	O2–C1–O1	121.47(19)
C3–C4	1.532(3)	O2–C1–C2	118.47(19)
C3–C2	1.536(3)	O1–C1–C2	120.01(19)
C3–C8	1.538(3)	N1–C3–C4	107.70(16)
C4–C5	1.530(3)	N1–C3–C2	107.31(17)
C8–C7	1.533(3)	C4–C3–C2	112.82(17)
C6–C7	1.522(3)	N1–C3–C8	109.70(17)
C6–C5	1.524(3)	C4–C3–C8	109.48(17)
		C2–C3–C8	109.75(17)
		C1–C2–C3	117.62(17)
		C5–C4–C3	112.32(17)
		C7–C8–C3	113.06(17)
		C7–C6–C5	111.95(18)
		C6–C7–C8	111.31(18)
		C6–C5–C4	111.11(19)

Symmetry transformations used to generate equivalent atoms: $i: -x+1, -y, -z+1$

[33]. However, only one of these Cu(II) complexes is square planar [34] as the coordination number of the Cu(II) atom in all the others is increased, mostly due to coordinated solvent molecule(s).

The bonds in the carboxylic group of ligand **L1** are clearly delocalized (see Table S2), while all other bond lengths are typical for single C–C and C–N bonds. The cyclohexyl ring is in a chair conformation. All three molecules of crystal water are involved in hydrogen bonds (Table S6), stabilizing the crystal structure. Each water molecule is in a typical tetrahedral environment provided by other water molecules, amine or carbonyl groups. Complex units in the structure form layers in the *bc* plane which are linked by hydrogen bonds from layers of crystal water in order to form an infinite 3D system (Fig. 3).

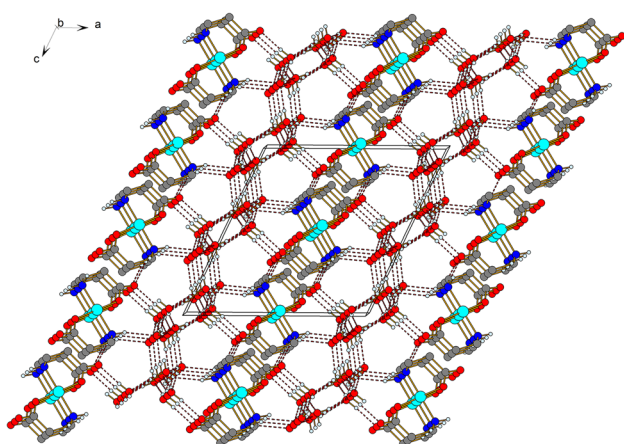


Fig. 3 Hydrogen bonds (dashed lines) forming a 3D supramolecular structure in **C1**. Hydrogen atoms not involved in hydrogen bonds are omitted for clarity

Interactions of the complexes with DNA

The kinetics of the interactions both complexes with calf thymus (CT) and herring testes (HT) DNA was investigated spectrophotometrically by following the change in absorbance at 260 nm as a function of time using stopped-flow spectroscopy. All measurements were taken at 7.2 and a temperature of 310 K. To keep a constant pH of 7.2, a PBS buffer was used for all measurements (PBS = phosphate buffer solution = 0.01 M, $c(\text{NaCl}) = 0.137$, $c(\text{KCl}) = 0.0027$ M, pH 7.4).

The substitution reactions of **C1** and **C2** with CT- and HT-DNA can be represented by Eq. (3):



where $\text{C} = \text{C1}$ or C2 ; $\text{DNA} = \text{CT-}$ or HT-DNA .

Here, k_2 is the second-order rate constant for the forward reaction, characterizing formation of the product, and k_1 is the rate constant for the reverse reaction. The rate of the reaction is then described by Eq. (4). All kinetic runs could be fitted by a single exponential function. Plots of k_{obsd} versus DNA concentration revealed a linear dependence with negligible intercept for both complexes. The values of the constants k_2 are listed in Table 2.

$$k_{\text{obsd}} = k_2[\text{P}] + k_1[\text{C}] \approx k_2[\text{P}] \quad (4)$$

Each *pseudo*-first-order rate constant, k_{obsd} , was calculated as the average of six or seven independent runs, and the values are given in Tables S2–S5. The experimental results for the substitution reactions of **C1** and **C2** with CT- and HT-DNA are shown in Fig. 4 (see also Figure S1 of the Supporting Information).

Table 2 Rate constants for the reactions of **C1** and **C2** with CT- and HT-DNA at pH = 7.2 (PBS buffer) and 310 K

	CT-DNA k_2 ($\text{M}^{-1} \text{s}^{-1}$)	HT-DNA k_2 ($\text{M}^{-1} \text{s}^{-1}$)
C1	$(3.8 \pm 0.1) \times 10^3$	$(6.3 \pm 0.2) \times 10^3$
C2	$(2.9 \pm 0.1) \times 10^3$	$(3.4 \pm 0.1) \times 10^3$

The results presented in Table 1 clearly show that the rate constants depend on the nature of the ligand in the complexes such that k_2 value for the reaction of **C1** has a greater value than that for **C2**. This can be attributed to the presence of the *tert*-butyl group on the ligand, which causes an increased steric effect for complex **C2**. Also, it can be seen that the reaction goes faster with HT-DNA than with CT-DNA.

DNA interaction studies

Electronic absorption spectroscopy is widely used to determine the DNA binding affinity of metal complexes. Hence, the potential binding abilities of **C1** and **C2** for CT- and HT-DNA were studied by UV spectroscopy. Typical titration curves for **C1** and **C2** in the presence of either DNA at different concentrations are given in Figs. 5 and S2; the other curves are similar and hence not given. Upon increasing the concentration of either DNA, a significant hyperchromic effect with the appearance of a new band at 258, 262 or 266 nm, but with only insignificant absorption changes in the region of 300–500 nm was observed, as shown in Fig. 5 (see also Figures S2, S3 and S4 in the Supporting Information). A significant hyperchromic shift with the appearance of a new signal in the UV–Vis spectra clearly suggests a strong interaction between the complexes and DNA [35, 36]. Moreover, the intrinsic binding constants K_b (Table 3) obtained for the two complexes with CT- and HT-DNA follow the order **C1** > **C2**. Once again, for complex **C2** the steric hindrance of the two *tert*-butyl groups results in a reduced interaction with DNA.

In order to further characterize of the binding of these complexes with DNA, competitive binding experiments were carried out on both EB-CT-DNA and EB-HT-DNA by varying the concentration of the complexes. EB is a planar cationic molecule emitting intense fluorescence at about 600 nm in the presence of DNA, due to its strong intercalation between adjacent DNA base pairs [37]. The enhanced fluorescence can be quenched upon the addition of a second molecule which can displace the EB and/or bound or break the secondary structure of the DNA [38]. The interactions of **C1** and **C2** with CT-DNA and HT-DNA were studied by monitoring the fluorescence intensity of EB in PBS buffer

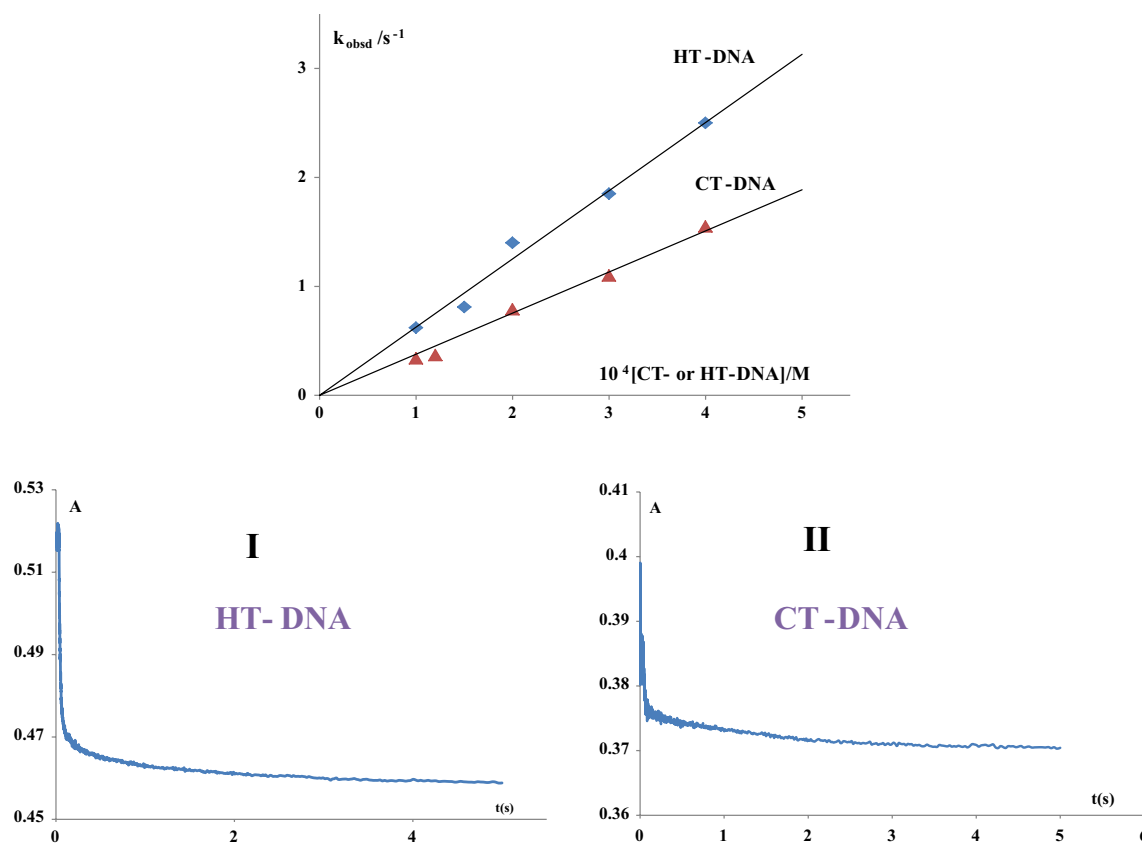


Fig. 4 Pseudo-first-order rate constants plotted as a function of CT- or HT-DNA concentration for the reactions between the complexes and DNA at pH=7.2 and 310 K in PBS buffer, $\lambda=260$ nm. Graph I—absorbance-time traces for the reaction between **C1** and HT-DNA

(2×10^{-4} M), pH=7.2, 310 K, PBS buffer; Graph II—absorbance-time traces for the reaction between **C1** and CT-DNA (2×10^{-4} M), pH=7.2, 310 K, PBS buffer

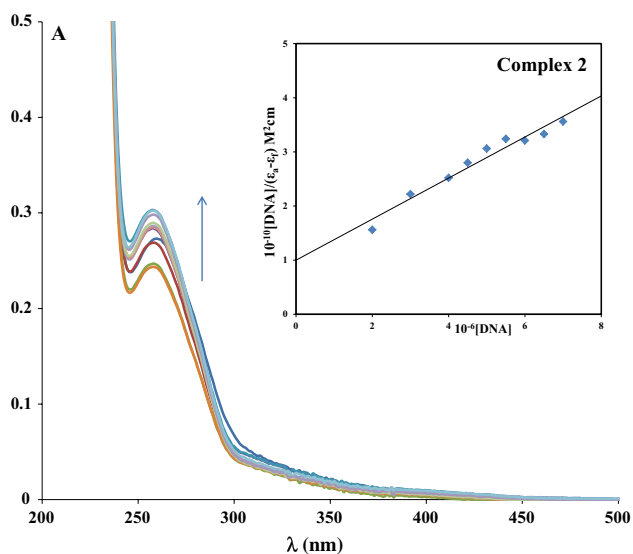


Fig. 5 UV-Vis titration spectra for complex **C2** (10 μM) in PBS buffer (phosphate buffer solution=0.01 M, $c(\text{NaCl})=0.137$, $c(\text{KCl})=0.0027$ M, pH 7.4) with increasing concentration of HT-DNA (0–10 μM). The arrow shows hyperchromism in the spectral band, $\lambda_{\text{max}}=258$ nm. Inset graph: plots of $[\text{DNA}] / (\epsilon_A - \epsilon_f)$ versus $[\text{DNA}]$

(pH=7.2). In all cases, there was significant quenching of fluorescence intensity due to the displacement of EB from the EB-DNA complex. The quenching parameters for the **C1** and **C2** were calculated using the Stern–Volmer equation. Increasing the concentration of **C1** or **C2** (0–10 μM) resulted in a significant decrease in EB fluorescence intensity, with a noticeable redshift (see Figs. 6 and S3, the other dependences are similar and are not given). These results indicate loss of EB from the EB-DNA complex due to displacement by complexes **C1** and **C2** [37, 39, 40].

The fluorescence intensity at 606, 609, 611 or 612 nm (depending on the complex-DNA combination) was used to estimate K_{sv} (Table 3). The fluorescence quenching data were also used to determine the number of binding sites (n) and the equilibrium binding constant K_{bin} by using the Scatchard equation [41–43];

$$\log(I_0 - I) / I = \log K_{\text{bin}} + n \log [Q]$$

The obtained values for K_{bin} and the number of binding sites (n) are given in Table S7. These values were calculated from plots of $\log(I_0 - I) / I$ versus $\log [Q]$ (see also Figure S4 in the Supporting Information; the other dependences are

Table 3 Binding constants for interactions of **C1** and **C2** with CT- and HT-DNA and BSA in PBS buffer

	Complex C1		Complex C2	
	K_b (M^{-1})	K_{sv} (M^{-1})	K_b [M^{-1}]	K_{sv} (M^{-1})
CT-DNA	$(5.9 \pm 0.1) \times 10^5$	$(9.8 \pm 0.1) \times 10^3$	$(3.8 \pm 0.1) \times 10^5$	$(9.6 \pm 0.1) \times 10^3$
HT-DNA	$(6.2 \pm 0.1) \times 10^5$	$(2.4 \pm 0.1) \times 10^4$	$(4.0 \pm 0.1) \times 10^5$	$(2.3 \pm 0.1) \times 10^4$
BSA	/	$(1.75 \pm 0.2) \times 10^5$	/	$(1.0 \pm 0.1) \times 10^5$

K_b = intrinsic binding constant; K_{sv} = Stern–Volmer constant; BSA = bovine serum albumin

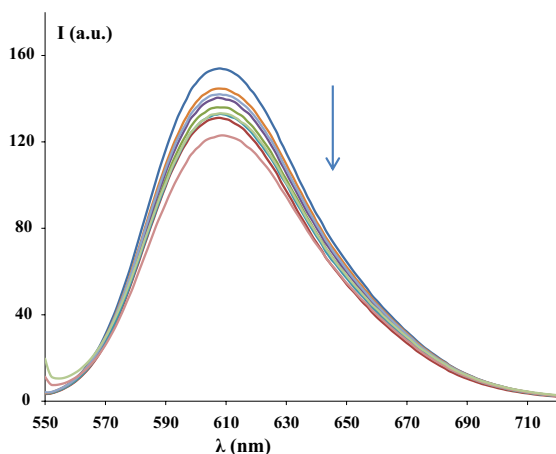
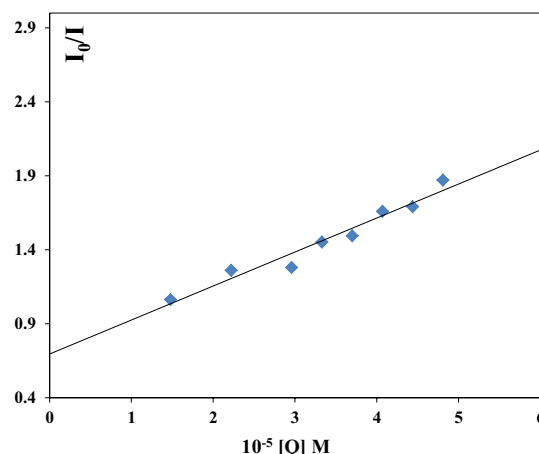


Fig. 6 Fluorescence titration spectra of EB-CT-DNA and of EtBr (10 μ M) bound to CT-DNA (10 μ M) in the presence of varying amounts of complex **C2**, λ_{max} = 609 nm. [The arrow shows changes



in fluorescence intensity upon increasing the concentration of **C2** (0–10 μ M).] Inset graph: Stern–Volmer plots for EB-DNA fluorescence titration with **C2**

similar and they are not given). The calculated number of binding sites is in a range from 0.8 to 1.5, hence approximately equal to 1, suggesting a single DNA binding site for both complexes.

According to the values of the constants presented in Table 3, a strong interaction of both complexes with CT- or HT-DNA is evident. Complex **C1** has a greater affinity for CT-DNA than complex **C2**, again due to greater steric effects for **C2**. To some extent, both complexes interact more strongly with HT-DNA than with CT-DNA, which can be attributed to the higher proportion of guanine bases in the former.

Viscosity measurements

Viscosity measurements were taken to further characterize the interactions of complexes **C1** and **C2** with CT-DNA. Classical intercalation results in lengthening and stiffening of the double helix of DNA, leading to an increase in viscosity [44, 45]. The addition of increasing amounts (up to $r=1.0$) of **C1** and **C2** to a CT-DNA solution (0.01 mM) resulted in an increase in the relative viscosity of CT-DNA (Figure S6), which was more pronounced upon the addition of **C1**. Therefore, the observed results suggest that the complexes bind to CT-DNA by intercalation.

Protein binding studies

Qualitative analysis of the binding of metal complexes to BSA can be performed by means of fluorescence spectroscopy, which can also provide useful information about the structure, dynamics and folding of proteins [46–48]. The changes in the fluorescence spectrum of BSA upon addition of different concentrations of complex **C1** or **C2** (0–10 μ M) in the range of 300–500 nm (λ_{ex} = 295 nm) are presented in Figs. 7 and S5 (The other dependences are similar and so not given.) The observed decrease in fluorescence intensity at 365 nm is indicative of an interaction between the complexes and BSA protein. Fluorescence quenching data were analyzed using the Stern–Volmer equation, and the quenching constant (K_{sv}) was calculated by using from a plot of I_0/I versus $[Q]$, as shown in Fig. 7.

The equilibrium binding constant K_{bin} and n (see also Table S7) as the number of binding sites can be analyzed by the Scatchard equation (see also Figure S7 of the Supporting Information, the other dependences are similar and so are not given). The values of n for the studied complex are 0.9 or 1.1 which strongly suggested the existence of a single binding site in BSA for these complexes.

According to the obtained constants, both complexes interact strongly with the BSA protein (Table 3). By

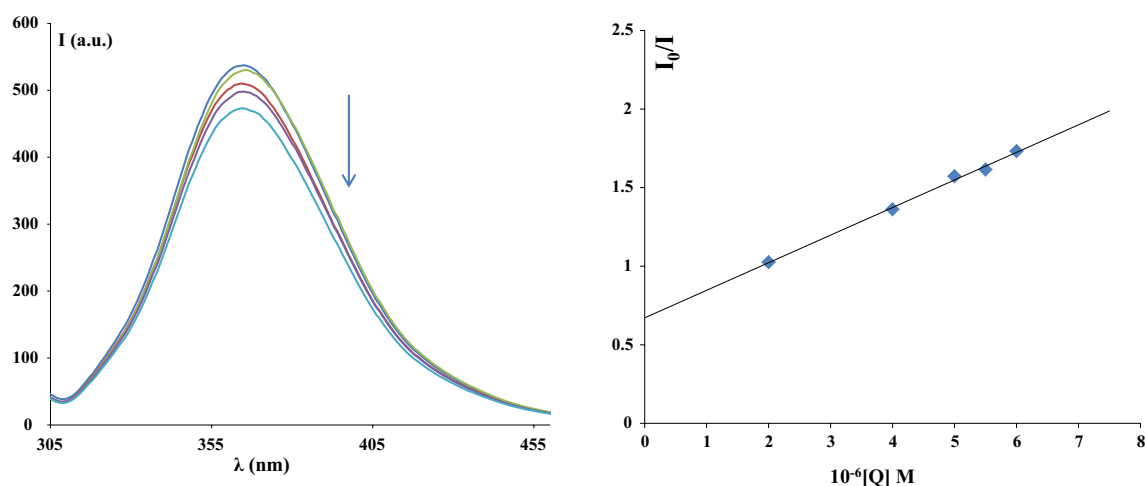


Fig. 7 Emission spectrum of BSA (10 μM ; λ_{ex} , 295 nm; λ_{em} 365 nm) in the presence of increasing amounts of **C1** (0–10 μM), $\lambda_{\text{max}}=365$ nm. The arrow shows the direction of emission intensity changes

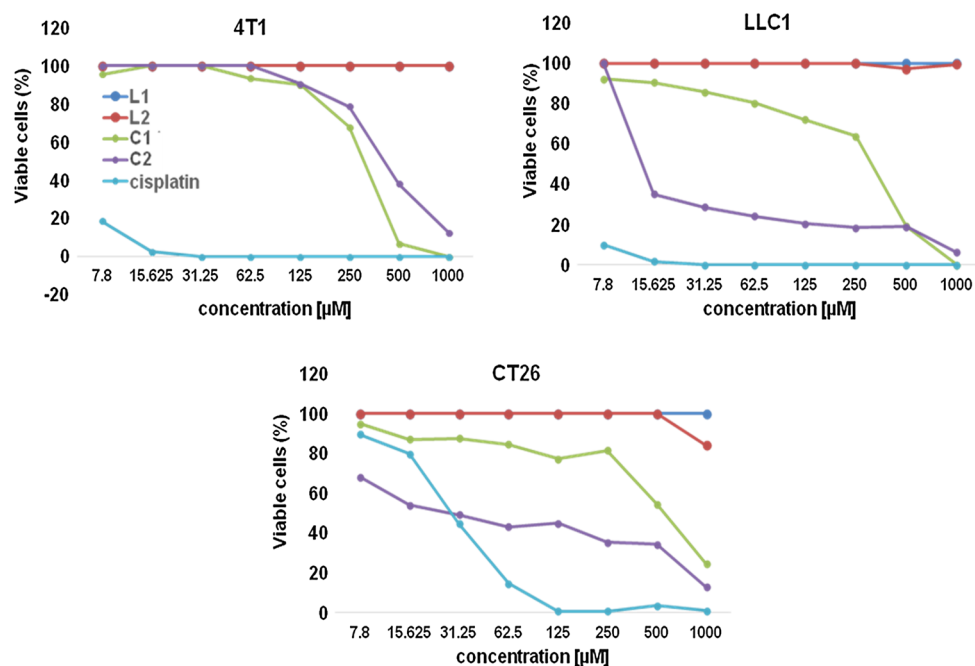
upon increasing the concentration of the complex. Inset graph: plots of I_0/I versus $[Q]$

comparing the obtained quenching constants (K_{sv}) for the interactions of complexes **C1** and **C2** with DNAs and BSA, it can be seen that studied Cu(II) complexes interact better with BSA than with DNA (Table 3). Furthermore, complex **C1** interacts more strongly with BSA than complex **C2**. The *tert*-butyl groups of **C2** most likely lead to steric hindrance, resulting in a weakened interaction with BSA. Similar results have been reported for other amino acid complexes [49, 50].

Anticancer activity of the complexes

The results of the MTT assays indicate that the free proligands **L1** and **L2** have no cytotoxic effect against the three tested carcinoma cell lines (CT26, 4T1, LLC1), even at a concentration of 1000 μM (Fig. 8). The cytotoxic effect of both copper complexes on all three cell lines proved to be dose dependent. The complexes showed almost no cytotoxicity on murine mammary carcinoma cells, 4T1, up to concentration of 125 μM (Fig. 8). Complex **C2** had better cytotoxic activity against murine lung cancer cell

Fig. 8 Representative graphs of 4T1, CT26 and LLC1 cell survival after 72 h cell growth in the presence of the copper complexes and free proligands



line, LLC1 and murine colon carcinoma cell line, CT26 cells than **C1** (Fig. 8). The cytotoxic effect of **C2** on LLC1 was lower compared to cisplatin (Fig. 8). However, lower percentages of viable CT26 cells were detected after exposure to **C2** at lower concentrations (7.8 and 15.625 μM) compared to the same concentrations of cisplatin (Fig. 8).

The analysis of IC_{50} values also indicates that complex **C1** has a lower cytotoxic effect against CT26 and LLC1 cell lines compared with the effect of **C2** (Table 4). Although the cytotoxic activity of **C2** toward murine lung carcinoma cells LLC1 is lower compared with cisplatin, the IC_{50} values for **C2** ($15.61 \pm 6.86 \mu\text{M}$) on LLC1 are relatively low.

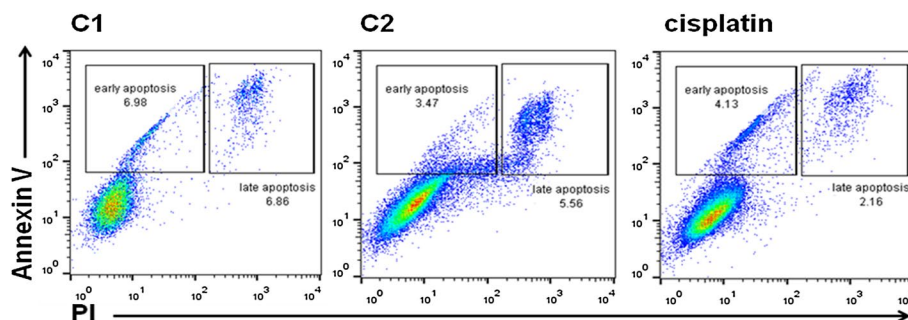
In order to determine the potential for induction of apoptotic death by the complexes, flow cytometry analysis of CT26 cells stained with Annexin V and PI after 24 h exposure to the complexes (concentration 15 μM) was carried out. The results indicate that after 24 h, both complexes induce apoptotic death of CT26 cells (Fig. 9). Moreover, both complexes had higher cytotoxic effects on CT26 compared to cisplatin (concentration 15 μM). These observations correlate with the MTT assays, which indicate better cytotoxic effects for the copper(II) complexes at lower concentrations on CT26 cells than cisplatin (15 μM).

Table 4 IC_{50} values (μM) for 72 h of action of the copper(II) complexes, free proligands and cisplatin on 4T1, CT26, and LLC1 cells, as determined by MTT assays

Compound	4T1	CT26	LLC1
C1	221.87 ± 16.25	655.42 ± 118.67	195.90 ± 33.05
C2	390.58 ± 56.48	39.86 ± 7.09	15.61 ± 6.86
L1	> 1000	> 1000	> 1000
L2	> 1000	> 1000	> 1000
Cisplatin	< 7.8	29.11 ± 5.87	< 7.8

Data are presented as mean values \pm SD (standard deviation) from three experiments

Fig. 9 Representative flow plots showing the percentages of early apoptotic, late apoptotic and viable CT26 cells after 24 h treatment the copper complexes (concentration: 15 μM)



Conclusion

Two new copper(II) complexes with β -amino acid ligands were synthesized and characterized. The ligand precursors are coordinated via nitrogen and oxygen atoms to the copper(II) center, giving square-planar structures as confirmed by X-ray analysis for complex **C1**. The interactions with calf thymus and herring testes DNA were studied by stopped-flow spectroscopy. Based on the obtained rate constants, it can be concluded that the reaction goes faster with HT-DNA than with CT-DNA, probably due to the higher percentage of guanine in the former. The interactions between the complexes and CT-DNA, HT-DNA and bovine serum albumin were also examined. Overall, both complexes have good affinities for the both CT- and HT-DNA. Complex **C1** has a greater affinity for DNA than **C2**, which can be explained by the steric effect of *tert*-butyl groups in **C2**. Viscosity measurements suggest that the complexes bind to CT-DNA by intercalation. According to the obtained quenching constants, it can be concluded that both copper(II) complexes interact more strongly with BSA than the DNA. We have also studied the antitumor activities of these complexes. In conclusion, it can be stated that copper(II) complex **C2** has a relatively low cytotoxic effect on murine mammary carcinoma cells, a moderate effect on murine carcinoma cells and a relatively high cytotoxicity toward murine lung cancer cells.

Supplementary data

CCDC 1810786 contains the supplementary crystallographic data for this paper. These data can be obtained free of charge via <http://www.ccdc.cam.ac.uk/conts/retrieving.html>, or from the Cambridge Crystallographic Data Centre, 12 Union Road, Cambridge CB2 1EZ, UK; fax: (+44) 1223 336 033; or e-mail: deposit@ccdc.cam.ac.uk.

Acknowledgements The authors are grateful to the Ministry of Science and Technological Development of the Republic of Serbia for financial support (Grants Nos. 172016, 172034, 175069, 175103, 172011) and Faculty of Medical Sciences for grant MP 2014/02. This work was

also supported by the project VEGA 1/0598/14. We thank prof. Ana Popović-Bijelić and prof. Miloš Mojović (EPR Lab, Faculty of Physical Chemistry, University of Belgrade) for acquiring and analyzing the EPR spectra.

References

- Tisato F, Marzano C, Porchia M, Pellei M, Santini C (2010) *Med Res Rev* 30:708–749
- Goodman VL, Brewer GJ, Merajver SD (2004) *Endocr Relat Cancer* 11:255–263
- Molina-Holgado F, Hider RC, Gaeta A, Williams R, Francis P (2007) *Biometals* 20:639–654
- Iakovidis I, Delimaris I, Piperakis SM (2011) *Mol Biol Int* 2011:594529
- Prudhomme M (2013) *Advances in anticancer agents in medicinal chemistry*. Bentham Science Publishers, Sharjah, p 256
- Gielen M, Tiekink ER (2005) *Metallotherapeutic drugs and metal-based diagnostic agents: the use of metals in medicine*. Wiley, New York, p 219
- Marzano C, Pellei M, Tisato F, Santini C, *Anticancer Agents* (2009) *Med Chem* 9:185–211
- Chohan ZH, Sumrra SH, Youssoufi MH, Hadda TB (2010) *Eur J Med Chem* 45:2739–2747
- Patil SA, Naik VH, Kulkarni AD, Badami PS (2010) *Spectrochim Acta A Mol Biomol Spectrosc* 75:347–354
- Shebl M, Khalil SM, Ahmed SA, Medien HA (2010) *J Mol Struct* 980:39–50
- Dhayabaran VV, Prakash TD, Renganathan R, Friehs E, Bahne-mann DW (2017) *J Fluoresc* 27:135–150
- Li A, Liu YH, Yuan LZ, Ma ZY, Zhao CL, Xie CY, Bao WG, Xu JY (2015) *J Inorg Biochem* 146:52–60
- Eslami Moghadam M, Saidifar M, Divsalar A, Mansouri-Torshizi H, Saboury AA, Farhangian H, Ghadamgahi M (2016) *J Biomol Struct Dyn* 34:206–222
- Jalilehvand F, Sisombath NS, Schell AC, Facey GA (2015) *Inorg Chem* 54:2160–2170
- Dharmaraja J, Subbaraj P, Esakkidurai T, Shobana S, Raji S (2014) *Acta Chim Slov* 61:803–812
- Tay WM, Epperson JD, da Silva GF, Ming LJ (2010) *J Am Chem Soc* 132:5652–5661
- Porter EA, Wang X, Lee H, Weisblum B, Gellman SH (2000) *Nature* 404:565
- Specker E, Bottcher J, Lilie H, Heine A, Schoop A, Muller G, Griebenow N, Klebe G (2005) *Angew Chem Int Ed* 44:3140–3144
- Myers AG, Barbay JK, Zhong B (2001) *J Am Chem Soc* 123:7207–7219
- Barry NP, Sadler PJ (2013) *Chem Commun* 49:5106–5131
- Ronconi L, Sadler JP (2007) *Coord Chem Rev* 251:1633–1648
- Lebedev AV, Lebedeva AB, Sheludyakov VD, Kovaleva EA, Ustinova OL, Kozhevnikov IB (2005) *Russ J Gen Chem* 75:1113–1124
- (2007) Oxford diffraction, CrysAlis CCD, CCD data collection GUI. Oxford Diffraction Ltd., Oxford
- Palatinus L, Chapuis GJ (2007) *Appl Crystallogr* 40:786–790
- Sheldrick GM (2015) *Acta Crystallogr Sect C Cryst Struct Commun* 71:3–8
- Farrugia LJ (1999) *J Appl Crystallogr* 32:837–838
- Brandenburg K (2009) DIAMOND (version 3.2i) Crystal Impact GbR. Bonn
- Meadows KA, Liu F, Sou J, Hudson BP, McMillin DR (1993) *Inorg Chem* 32:2919–2923
- Mosmann T (1983) *J Immunol Methods* 65:55–63
- Sarker SD, Nahar L, Kumarasamy Y (2007) *Methods* 42:321–324
- Schoenberg LN, Cooke DW, Liu CF (1968) *Inorg Chem* 7:2386–2393
- Swaminathan K, Busch DH (1961) *J Inorg Nucl Chem* 20:159–163
- Groom CR, Bruno IJ, Lightfoot MP, Ward SC (2016) *Acta Crystallogr B* 72:171–179
- Kamwaya ME, Teoh SG, Fiz J (1984) *Malaysia* 5:1–7
- Koumoussi ES, Zampakou M, Raptoulou CP, Psycharis V, Beavers CM, Teat SJ, Psomas G, Stamatas TC (2012) *Inorg Chem* 51:7699–7710
- Rizvi MA, Zaki M, Afzal M, Mane M, Kumar M, Shah BA, Srivastav S, Srikrishna S, Peerzada GM, Tabassum S (2015) *Eur J Med Chem* 90:876–888
- Meyer-Almes FJ, Porschke D (1993) *Biochemistry* 32:4246–4253
- Patra A, Sen TK, Ghorai A, Musie GT, Mandal SK, Ghosh U, Bera M (2013) *Inorg Chem* 52:2880–2890
- Liu ZC, Wang BD, Yang ZY, Li Y, Qin DD, Li TR (2009) *Eur J Med Chem* 44:4477–4484
- Howe GM, Wu KC, Bauer WR (1976) *Biochemistry* 19:4339–4346
- Karsten Rippe BIF (1997) *Futura* 12:20–26
- Qu X, Chaires JB (2000) *Methods Enzymol* 321:353–369
- Raja DS, Bhuvanesh NSP, Natarajan K (2011) *Inorg Chem* 50:12852–12866
- Li DD, Tian JL, Gu W, Liu X, Yan SP (2010) *J Inorg Biochem* 104:171–179
- Jiang M, Li YT, Wu ZY, Liu ZQ, Yan CW (2009) *J Inorg Biochem* 103:833–844
- Ramachandran E, Thomas SP, Poornima P, Kalaivani P, Prabhakaran R, Padma VV, Natarajan K (2012) *Eur J Med Chem* 50:405–415
- Paitandi RP, Gupta RK, Singh RS, Sharma G, Koch B, Pandey DS (2014) *Eur J Med Chem* 84:17–29
- Miller JN (1979) *Proc Anal Div Chem Soc* 16:203–208
- Annaraj B, Balakrishnan C, Neelakantan MA (2016) *J Photochem Photobiol B* 160:278–291
- Theetharappan M, Subha L, Balakrishnan C, Neelakantan MA (2017) *Appl Organomet Chem* 31:1–19